4.1 Introduction

In the previous chapter, we tried to settle the room temperature crystal structure of nano powder of BF-0.50PT using high energy synchrotron x-ray powder diffraction data.The nano-structured magnetic materials differ significantly from their bulk counterparts and have been exploited for several technological applications. The nanostructured ferromagnetic (FM) and ferrimagnetic (FerM) materials are commonly used in permanent magnets, magnetic data storage, logic devices, ferrofluids, biomedical devices etc. [Dormann et al. (1997),(1992), Fiorani (2005), Pankhurst et al. (2003)]. In recent years, nanostructured antiferromagnetic (AFM) materials have also received considerable attention for applications like spin valves, magnetic random access memory and AFM and FM composite based hard magnets [Mørup et al. (2007)].The tetragonal phase of BF-xPT has got several unusual characteristics : (1) it shows anomalously huge tetragonality (η= (c/a -1)) that is more than three times that of the commercial MPB ceramics like PZT, (2) tetragonality increases on approaching the MPB and becomes ~ 18.73% for x=0.31 whereas it decreases on approaching the MPB in PZT,(3) the high tetragonality phase does not result from the paraelectric (PE) cubic phase directly but by an isostructural phase transition from a low η phase, which gets formed first from the cubic paraelectric phase, below the curie temperature (4) and it shows very low T_N **(** ~ 209K for x=0.31**)** as compared to neighbouring monoclinic compositions with T_N ~ 473 K for x=0.27. Finite size effects in AFMs nanoparticles, nanorods and thin films have been investigated extensively [Molina-Ruiz et al. (2011), Kodma et al. (1996), Ambrose et al.(1996), Tang et al. (2003), Weschke et al. (2004)] and it has been shown that T_N decreases with decreasing particle size or the thin film thickness as per the predictions of Néel[Selbach et al. (2007)]. The decrease in T_N is found to be consistent with Binder's scaling theory of

critical phenomena in reduced dimension systems which give the following universal power law dependence of transition temperature [Binder (1972)].

$$\frac{T_N^b - T_N^{grain}}{T_N^b} = \left(\frac{d}{\xi_0}\right)^{-(1/\nu)} \quad \text{.....(4.1)}$$

where T_N^b and T_N^{grain} are the bulk and finite size AFM transition temperatures, d is the grain diameter, ξ_0 is the magnetic correlation length at 0 K and ν the critical exponent related to ξ.

4.2 Experimental

The different sizes of BF-0.5PT samples were synthesized by the methods discussed in chapter II. High energy synchrotron x-ray powder diffraction data were analysed by Rietveld method using the FULLPROF software package [Carvajal (1993)], discussed in chapter III. Magnetic characterization was carried out using a Quantum Design® Evercool II PPMS®. Magnetization vs temperature measurements were performed in the temperature range of 2.5K-390K in an applied field of 5000 Oe or 500 Oe on case to case basis, whereas magnetization vs applied field measurements were performed at selected temperatures up to a maximum field of 7 Tesla. Neutron powder diffraction measurements were carried out on high-resolution powder diffractometer SPODI at FRM-II, Garching, Germany. The incident neutron wavelength was 2.5367 Å. Approximately 10 g of the sample, contained in a cylindrical niobium holder with 50 μm wall thickness, 40 mm height, and 10 mm diameter, was used for these measurements. The data were collected at steps of 0.05° in the 2θ range from 1 to 157°. A closed cycle cryostat was used for sample temperature variation in the temperature range of 4 K to 500 K

4.3 Rietveld analysis of the neutron powder diffraction pattern

Neutron powder diffraction data were analyzed by Rietveld refinement technique using FULLPROF software package [Carvajal (2010)]. The magnetic structure is based on the propagation vector and the chemical unit cell which reveals the relation between moment orientations in the magnetic sub lattice. Representation theory is used to find out the possible magnetic structures and these structures are decomposed into irreducible representations (IR) of the little group G_k, which leave the propagation vector, k, invariant. G_k is a subgroup of the chemical space group G_0.The moment of a particular magnetic ion, say jth, can be written as a Fourier expansion

$$m_j = \sum_k \psi_j^k \exp\{-2\pi i k.r_j\} \quad \text{.....(4.2)}$$

where vector r_j represent the position of the jth magnetic ion. The general basis vector ψ_j^k is made up from contributions from several basis vectors, the ψ_ns , corresponding to a particular IR of G_k and can be written as,

$$\psi_j^k = \Sigma\, c_n \psi_n \quad \text{.....(4.3)}$$

where c_ns are the mixing coefficients.

For tetragonal magnetic structure representation of the Fe sublattice (1b site) at k= ½, ½, ½ can be expressed in terms of two IRs

$$\Gamma^{1b} = \Gamma_3 + \Gamma_5 \quad \text{.....(4.4)}$$

Where Γ_5 is two dimensional and Γ_3 is one dimensional. Refinement with the two models (Γ_3 and Γ_5) shows that the second IR (Γ_5) gives better fit [Bhattacharjee et al (2010)]. Basis vector of Γ_1 gives a G-type of antiferromagnetic structure with the magnetic moments along the crystallographic c axis. There are two basis vector for Γ_5 and the

combined structure with these two basis vectors are again of G-type but with the magnetic moment in the ab plane. The character table and the basis vectors of these two IRs of the tetragonal phase are given in Table 4.1

Table 4.1 Character table and basis vector (magnetic) of space group P4mm at k = (1/2, 1/2, 1/2)

Irreducable Representation	Symmetry elements (Kovalev)							
	{1|000}	{2_00z|000}	{4+_00z|000}	{4-_00z|000}	{m_x0z|000}	{m_0yz|000}	{m_x-z|000}	{m_xxz|000}
Γ_1	1	1	1	1	1	1	1	1
Γ_2	1	1	1	1	-1	-1	-1	-1
Γ_3	1	1	-1	-1	1	1	-1	-1
Γ_4	1	1	-1	-1	-1	-1	1	1
Γ_5	1 0 0 1	-1 0 0 -1	i 0 0 -i	-i 0 0 i	0 1 1 0	0 -1 1 0	0 –i i 0	0 i -i 0

Irreducable Representation	**Basis vector**	**1b site**	
		(1/2,1/2,z)	
Γ_3	$\tau_{1,1}$	Re Im	(0 0 1)
Γ_5	$\tau_{5,1}$	Re Im	(0 0 1) (0 0 1)
	$\tau_{5,2}$	Re Im	(0 0 1) (0 0 1)

4.4 Result and diacussion

4.4.1 Magnetization studies of BF-0.5PT powder

BF-0.5PT with average particle sizes of ~ 18, 31, 45 and 120 nm are selected for the magnetic studies. [Details are given in Chapter II and III].Temperature (T) dependence of magnetization (M) of BF-0.50PT was investigated at a magnetic field of 5000 Oe during heating in the temperature range of 2K to 390 K for 120 nm, 45 nm, 31 nm and 18 nm size powders in zero-field cooled (ZFC) and field cooled (FC) modes . The results are shown in fig.4.1 (a to d). In M(T) of curves BF-0.5PT, the magnetization starts increasing below a certain temperature with decreasing temperature like in ferromagnetic, ferrimagentic [Cullity (1972)] or canted antiferromagnetic system. Therefore, the behaviour of M(T) curve of BF-0.5PT is probably due to canted antiferromagnetic ordering in which the weak ferromagnetic component appears below the magnetic transition temperature. The ZFC M-T plot of the 120 nm size particles shows a Néel transition temperature T_N ~ 120K (see the inset also) similar to that reported in bulk powders of BF-0.5PT [Binder (1972)]. Intriguingly, on reducing the particle size to 45 nm, 31 and 18 nm, the Néel temperature increases drastically to 230, 250 and 350K, respectively, as can be seen from various insets to Fig 4.1. The anomaly at T_f ~17K in the ZFC M-T plot of the bulk is known to be due to spin glass freezing [Zhu et al. (2008)].

$BiFeO_3$ shows linear M-H curve because of the presence of the spatially incommensurate modulated spiral spins structure of approximate wavelength of 62 nm [Lebeugle et al. (2007)]. In this scenario, one expects weak ferromagnetism due to spin canting in the shell region of the 18 nm size nanoparticles of BF-0.5PT as observed in similar core-shell type systems in non multiferroic AFM oxides [Benitez et al. (2008).

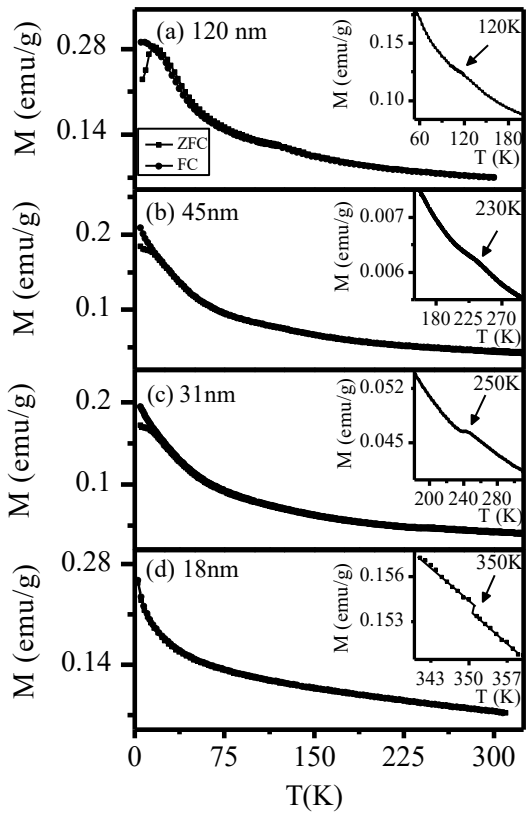

Fig.4.1 The temperature dependence of the FC and ZFC magnetizations of BF-0.5PT: (a–d) 120, 45, 31 and 18 nm size powders under magnetic field of 5000 Oe, The insets of (a to d) depict magnified plot near T_N

This was confirmed by the M-H measurements, the results of which are shown in Fig 4.2. It is evident from Fig 4.2(a) that the M-H plots for 120 nm, 45 nm and 31 nm size powders are straight lines confirming their paramagnetic nature at room temperature, whereas the 18 nm size particles exhibit nonlinear M-H curve, with a little loop opening. With decreasing temperature, the M-H loop of 18 nm size particles opens up further as can be seen from the two insets of Fig 4.2(b) which compare the M-H plots for 18 nm size particles at 300 K and 5 K. Further, the M-H loop in Fig 4.2(b) inset reveals an exchange bias (E_B) of ~ 337 Oe at 5K, which decreases with increasing temperature for the same particle size. The E_B decreases with increasing particle size also for the same

temperature. For example, the E_B at 5 K is ~17 Oe and ~8 Oe for 31 nm and 45 nm size powders, respectively, while it is absent for the bulk powder (see Fig 4.2(c) inset).

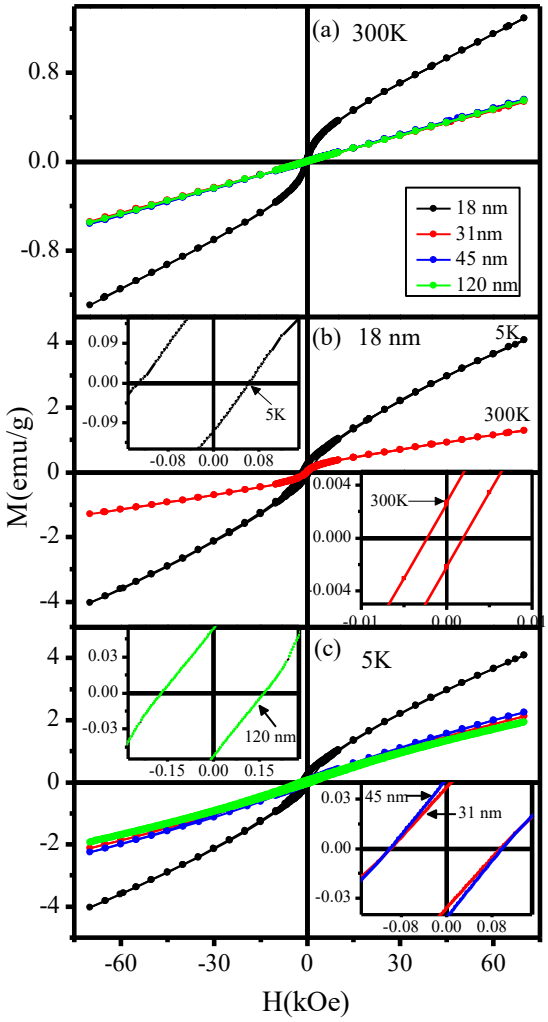

Fig.4.2 M-H plots for (a)18, 31, 45,120 nm size powders at 300K, (b) 18 nm particles at 300 and 5K and (c) 18, 31, 45, 120 nm size powders at 5K. Insets of (b) and (c) compare exchange bias at 5K and 300K for 18 nm, and at 5K for 120 and 31 nm powders.

The more pronounced E_B, as shown in the inset of Fig 4.2(b), in the smallest size particles (~18 nm) is due to higher surface to volume ratio of 18 nm particles leading to more number of spins in the surface layers constituting the shell region.

To verify the exchange bias which is present in nano sample, we again capture the M-H measurement using the Quantum Design Evercool MPMS3 to a very close step size of 20Oe at room temperature. As shown in fig. 4.3 hysteresis loops were measured in both the zero-field-cooling (ZFC) and field-cooling (FC) condition. After being cooled in a magnetic field of $\pm 5T$ we observe that, there is a corresponding shift in the hysteresis loop in both horizontal and vertical FC hysteresis curve.

Upon cooling the sample in positive magnetic field results in a negative shift of the hysteresis loop and vice versa. A exchange bias with a value of ~328 Oe is detected from the shift along the field axis of the FC curve which is approximately same as found by earlier result. The interface between the FM component of the canted spins in the shell region and the collinear AFM spins in the core (of BF-0.50PT) is responsible for the exchange bias effect as observed in other systems also [Benitez et al. (2008), Yusuf et al. (2013), Manna et al. (2014). Thus our M-H plot showing E_B effect not only confirms the coexistence of AFM and weak FM ordering but also reveals that they arise from a core-shell type of nanostructure of individual nanoparticles.

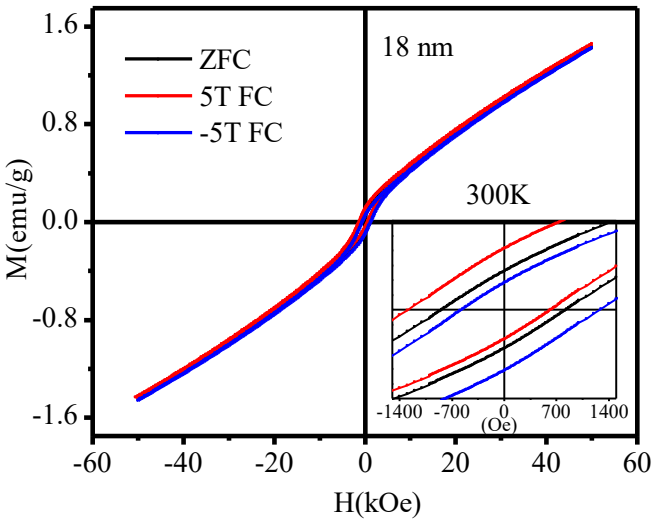

Fig.4.3 The field-dependent magnetization hysteresis (M-H) loops of BF-0.5PT of size 18nm. Inset shows the shifting of curve with fields.

4.4.2 Neutron diffraction studies

In order to realize the arrangement of magnetic moments in iron sublattice below T_N, powder neutron diffraction studies have been carried out in temperature range from 4K to 300K for nano and 4K to 460K for bulk powder. The temperature evolution of the magnetic peak corresponding to propagation vector k=½ ½ ½ in the neutron powder diffraction patterns is shown in Figs 4.4 (a) and 4.4(b) for bulk and 18nm size powders, respectively in the 2θ range from 30 to 38 degrees. The magnetic peak occurring just before the psuedocubic (100) nuclear peak is due to the antiferromagnetic ordering of the spin. The intensity of peak decreases with increasing temperature but does not become zero at T_N. In the bulk samples, the AFM peak (marked with asterisk in the figure) appears below T_N ~120K whereas it is present even at room temperature in 18nm size powder.

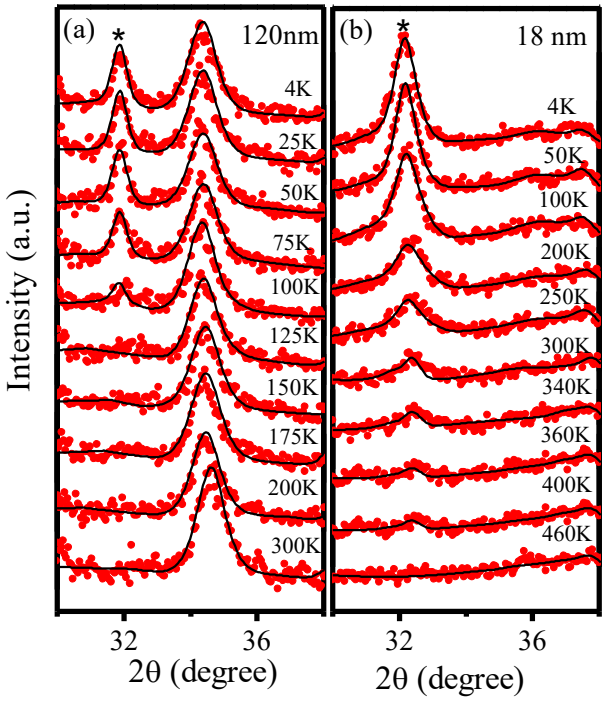

Fig. 4.4 Temperature dependent powder neutron diffraction profile of bulk and nano BF-0.5PT samples. Corresponding temperatures are shown in figures.

This clearly shows a drastic enhancement of T_N in 18nm size powder. The variation of the integrated intensity of the ½ ½ ½ magnetic peak with temperature shown in Fig 4.5 (a) reveals T_N ~120K in agreement with the T_N determined from ZFC M-T measurements (Fig. 4.1). The magnetic neutron peaks of 18 nm particles have sharp and diffuse (broad) components (see Fig 4.5(b) which depicts two deconvoluted Lorentzians) linked with the coexisting high and low tetragonality phases, respectively, as confirmed by Rietveld refinements using SXRPD data (see chapter III). The diffuse component of the magnetic scattering is dominant above 250K. The variation of the integrated intensity of the sharp component with temperature for 18nm size powder shows a linear behaviour upto ~250K and its extrapolation to zero intensity gives a T_N of ~350 K in agreement with the M(T) results. Thus there is a drastic enhancement of T_N with respect to T_N =120K of the bulk

powder. The diffuse component shows temperature dependence different from that of the sharp component and the corresponding T_N is still higher, as small residual intensity can be seen at the AFM peak position even in 360 and 400 K profile in Fig. 4.5 (b). We propose that the diffuse component of the magnetic peak with shorter correlation length is due to spin disorder in a thin shell region of the surface layers of the nanoparticles. In this scenario, one expects weak ferromagnetism due to spin canting in the shell region of the 18 nm size nanoparticles of BF-0.5PT as observed in similar core-shell type systems in non multiferroic AFM oxides [Benitez et al. (2008)]. This weak ferromagnetism should be present even at room temperature as the corresponding T_N is well above the room temperature for 18 nm size particles.

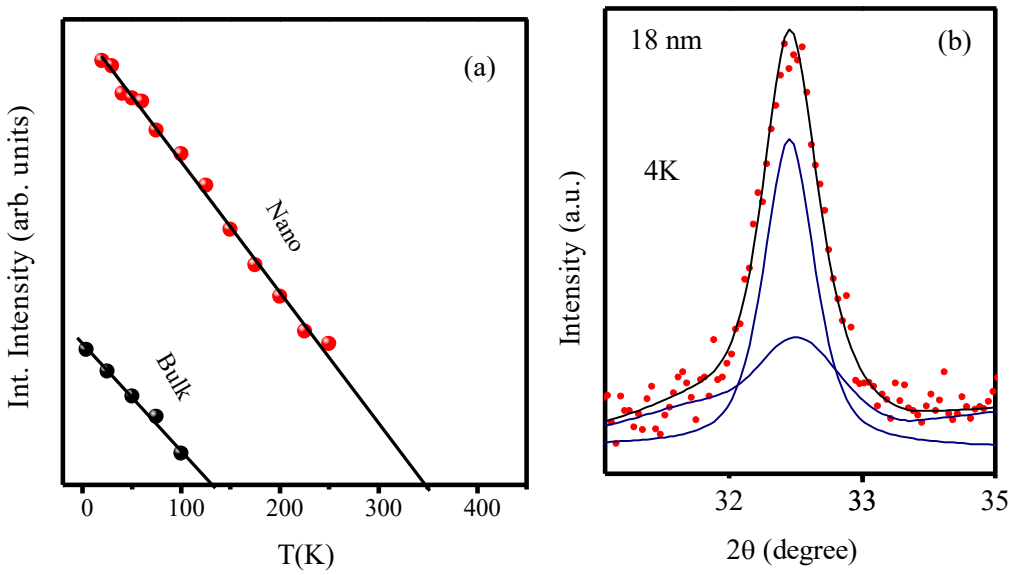

Fig. 4.5 (a) Variation in the integrated intensity of the magnetic peak with temperature for bulk and nano size powders. Dots represent measured data points, while the continuous line corresponds to the least-squares fitted Lorentzian(s). (b) Deconvolution of the magnetic peak of 18 nm size powder showing two different magnetic correlation lengths (ξ).

4.4.3 Role of super exchange interaction

The enhancement of T_N with size reduction is unique to MFAFMs. It is a consequence of the subtle interplay between the ferroelectric distortion and the strength of the superexchange interaction in the multiferroic BF-0.5PT. Table 4.2 lists the lengths of Fe^{3+}- O^{2-} bond lengths in the [001] direction for the bulk and the 18 nm size powder, as calculated using the positional coordinates obtained by Rietveld refinement of SXRPD patterns [see chapter III]. The longer Fe^{3+}- O^{2-} bond length (labelled as Fe-O_{1b} in Table 4.2) in the bulk powder is too big (2.571 Å) as compared to the sum of the ionic radii of Fe^{3+} and O^{2-} (~2.045 Å) to have any orbital overlap required for superexchange interactions in [001] direction in the bulk powders. As a result, the AFM superexchange interaction pathways are confined to [100] and [010] directions only.

Table 4.2 Fe-O bond lengths (Å of the dominant phase constituting the core of BF-0.5PT samples as a function of particle size

Size (nm)	Bond length (Å)		
	Fe-O_{1a}	Fe-O_{1b}	Fe-O_2
18	1.787	2.348	2.013
31	1.790	2.369	1.970
45	1.792	2.460	1.973
120	1.822	2.571	1.968

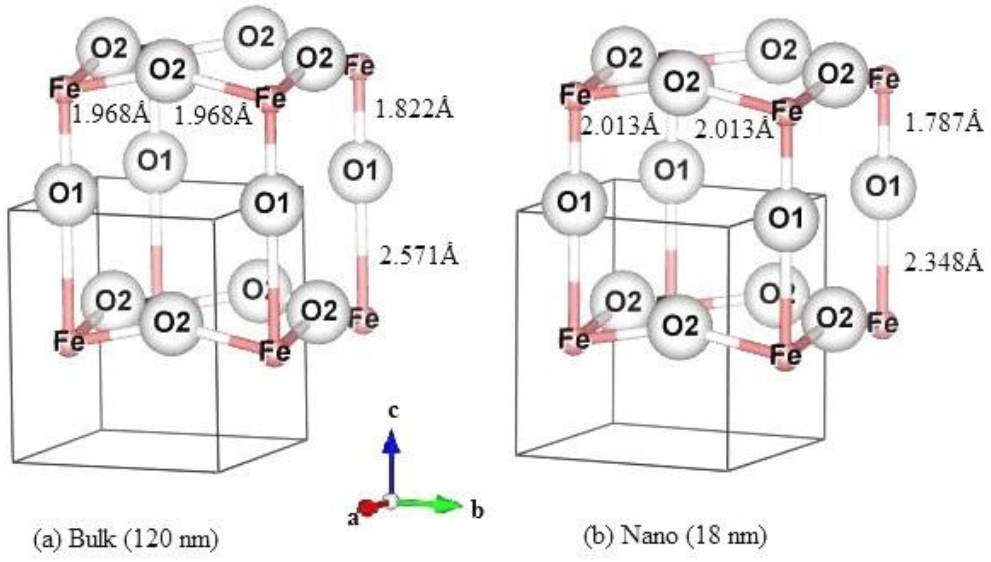

Fig.4.6 Fe-O-Fe exchange pathways (a) Bulk (b) 18 nm of $BiFeO_3$-0.50$PbTiO_3$

As the longer Fe^{3+}- O^{2-} bond in the [001] direction decreases systematically with particle size reduction (see Table 4.2 for bond length of the 18 nm size powder), there is a gradual enhancement of superexchange interaction in the [001] direction also. This crossover from essentially 2d AFM interactions in the bulk powders to 3d AFM interactions in nanoparticles of BF-0.50PT is responsible for the drastic rise in the T_N as a result of size reduction. Fig.4.6 shows the superexchange percolating path of Fe-O-Fe for bulk and nano sample of BF-0.5PT, for the better understanding of this system.

Thus, the physics of size effect in multiferroic AFM systems is entirely different from that in conventional AFM systems.

4.4.4 Evidence of enhancement of T_N at atomic level:

Although the XRD study shows that presence of two tetragonal phases in nano BF-0.5PT samples at room temperature. Temperature dependent neutron diffraction study was carried out for 18 nm size samples not only answer to structural information but also precisely determine the oxygen coordinates which is not possible through XRD data. It is

already well established refinement for bulk sample of BF-0.31PT [Bhattacharjee et al.(2010)], so our focus to visualized it nano part of this composition.

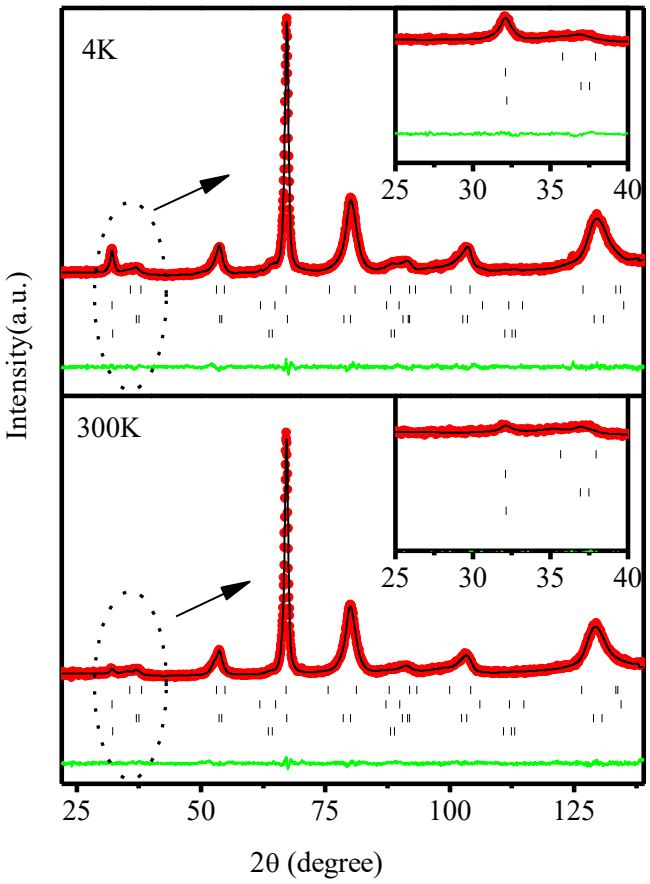

Fig. 4.7 Observed (dotted), calculated (continuous line) and difference profiles (bottom line) obtained from Rietveld refinement of BF-0. 5PT using P4mm space group. The inset shows the magnetic peak of nano powder at temperature of 4K and 300K.

We carried out Rietveld refinements for the BF-0.5PT sample having lowest particle size (~18 nm). Fig.4.7 shows neutron pattern at temperature of 4K and 300K. The parameter obtained from refinement is listed in table 4.3

Table 4.3 Rietveld refined positional coordinates, thermal parameters and lattice parameters of 18 nm size powder of BF-0.50PT at 4K and 300K. The magnetic R-factor for the coexisting phase is rather high due to the diffuse nature of the neutron peak component.

BF0.5PT with size 18 nm		Fractional coordinates				Thermal Parameters ($Å^2$)	Lattice Parameters (Å)	Statistical parameters
		Atom	x	y	z			
4K	Tetragonal phase-1	Bi/Pb	0.0	0.0	0.0	$B_{11}=B_{22}$= 0.146(4), B_{33}=0.183(9)	a=b= 3.9075(4) c= 4.129(1)	R_p= 10.0 R_{wp}= 9.49 R_{exp}= 7.37 χ^2 = 1.659 Magnetic R-factor: 1.27
		Fe/Ti	0.5	0.5	0.509(3)	B_{iso}=1.8(2)		
		O1	0.5	0.5	0.121(2)	$B_{11}=B_{22}$= 0.019(6) B_{33}= 0.05(1)		
		O2	0.0	0.5	0.649(1)	$B_{11}=B_{22}$= 0.091(5) B_{33}= 0.070(6)		
	Tetragonal phase-2	Bi/Pb	0.0	0.0	0.0	$B_{11}=B_{22}$= 0.028(2), B_{33}=0.005(3)	a=b= 3.9458(2) c= 4.0026(5)	
		Fe/Ti	0.5	0.5	0.599(2)	B_{iso}=1.6(1)		
		O1	0.5	0.5	0.056(2)	$B_{11}=B_{22}$= 0.052(2), B_{33}= 0.00006(1)		
		O2	0.0	0.5	0.576(1)	$B_{11}=B_{22}$= 0.005(3), B_{33}= 0.140(4)		
300K	Tetragonal phase-1	Bi/Pb	0.0	0.0	0.0	$B_{11}=B_{22}$= 234 (3), B_{33}= 0.073(9)	a=b= 3.9010 (5) c= 4.1442 (3)	R_p= 9.52 R_{wp}= 8.89 R_{exp}= 7.11 χ^2 = 1.56 Magnetic R-factor: 2.21
		Fe/Ti	0.5	0.5	0.512 (9)	B_{iso}= 1.848 (3)		
		O1	0.5	0.5	0.120 (1)	$B_{11}=B_{22}$ 0.045(6) B_{33}= 0.006 (1)		
		O2	0.0	0.5	0.651 (6)	$B_{11}=B_{22}$= 0.17 (2) B_{33}= 0.15 (2)		
	Tetragonal phase-2	Bi/Pb	0.0	0.0	0.0	$B_{11}=B_{22}$= 0.050(2), B_{33}= 0.005(7)	a=b= 3.9484 (3) c= 4.0079 (2)	
		Fe/Ti	0.5	0.5	0.605 (2)	B_{iso}=1.8(1)		
		O1	0.5	0.5	0.038 (2)	$B_{11}=B_{22}$= 0.041 (2), B_{33}= 0.0009 (1)		
		O2	0.0	0.5	0.555 (3)	$B_{11}=B_{22}$= 0.0002 (3), B_{33}= 0.15 (4)		

As far as the magnetic structure of BF-0.5PT is concerned, there is only one magnetically active cation, Fe^{3+}, in this solid solution and the magnetic structure therefore corresponds to the arrangement of magnetic moments of Fe^{3+} sublattice only. The unit cell volume shows a small but distinct change around 350 K (see Fig.4.8). The temperature ~350 K at which we observe anomalies in the tetragonal unit cell volume, coincides with the magnetic transition temperature T_N ~350 K obtained by the magnetization studies. These

anomalies in the unit cell parameters at T_N reveal the presence of magnetoelastic coupling in BF-0.50PT. There is another isostructural phase transition across T_N was observed which is obtained by Rietveld refinement of nano sample.

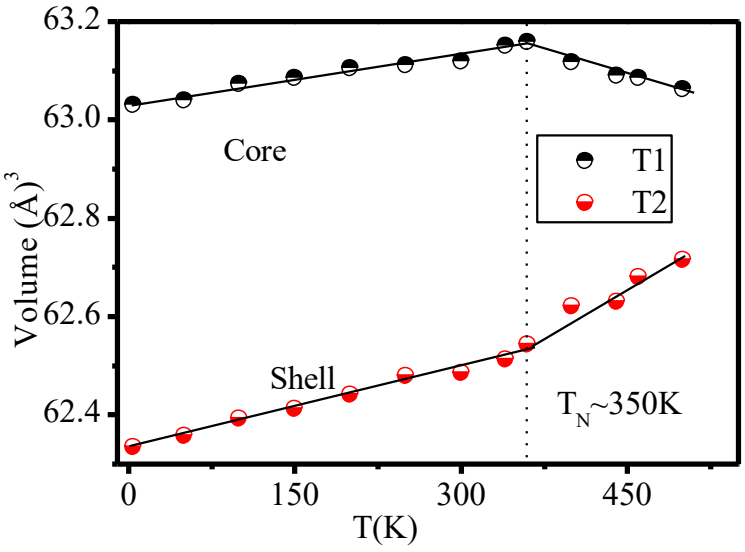

Fig. 4.8 Temperature dependent variation of unit cell volume obtained by powder neutron diffraction profile of 18nm BF-0.5PT samples.

Isostructural phase transition (IPT) are very rare [Ranjan et al (2005)] but have been reported across T_N in another multiferroics $LuMnO_3$ and $YMnO_3$ [Lee et al (2008)] recently but at very low temperatures. More recently, an isostructural phase transition has also been reported in the (1-x)$BiFeO_3$- x$PbTiO_3$ system at high temperatures close to ferroelectric phase transition rather than magnetic transition temperature [Bhattacharjee et al. (2011)].

The variation of the ordered magnetic moment per Fe^{3+} ion, obtained by Rietveld refinements, as a function of temperature in the range 2-340 K is shown in Fig.4.9. The ordered moment were fitted by power law $\mu(T) = \mu_0(1-T/T_N)^{\beta}$ using μ_0, T_N and β as fitting parameters for the data 2K<T<350 K. The fits are shown as solid lines through the data

points. The fits give β = 0.41(3) and T_N~ 350(5) from the ordered moment curve. The value of critical exponent β obtained from calculated ordered magnetic moment data is close to half which suggests that the antiferromagnetic phase transition may be second order in nature.

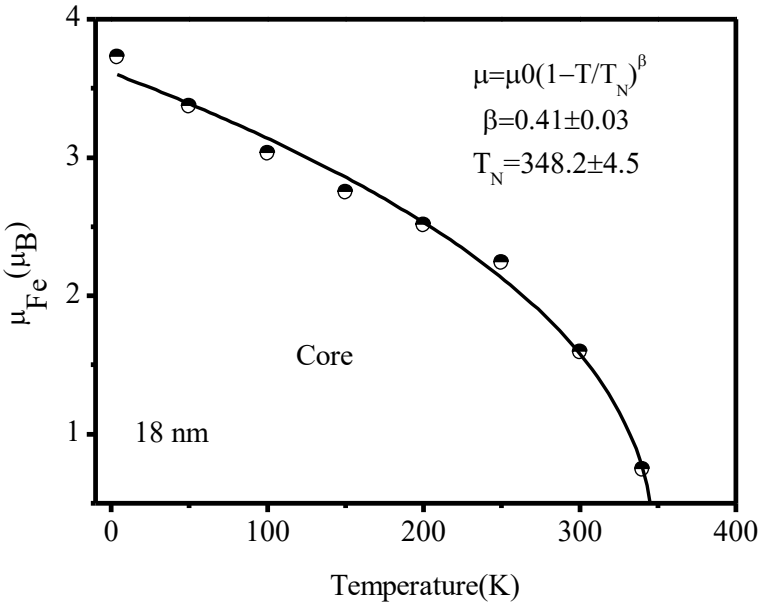

Fig. 4.9 Temperature dependence of ordered magnetic moment (half filled circle) obtained from the Rietveld refinement of neutron powder diffraction data fitted curve with $\mu(T) = \mu_0(1\text{-}T/T_N)^{\beta}$

4.5 Summary and conclusions

The main conclusions of this chapter may summarized as under:

(1) The Néel temperature (T_N) of BF-0.5PT where increases from ~120K in bulk powders to ~350K in 18nm size ferroelectric powders. It is possible to raise the Néel temperature (T_N) substantially (upto ~ 200K) through particle size reduction. This extraordinary enhancement of T_N is linked with the tunablity of the strength of the superexchange interaction through a decrease in the ferroelectric distortion in low dimensional systems due to finite size effects.

(2) The nano sample also shows a huge amount of exchange bias (E_B) of ~ 337 Oe at 5K, which confirms core-shell type structure.

(3) There is significant shift in the lattice parameter obtained from Rietveld refinement of the nuclear and magnetic structures using neutron powder diffraction data at magnetic transition temperature without affecting the symmetry.

The magnetic properties towards the $BiFeO_3$ end of MPB for bulk samples shows variety of exotic phenomenon like spin reorientation temperature, sudden increase in the Neel transition temperature after crossing the boundary. The size plays an important role in magnetic properties of BF-0.50PT samples. It will be interesting to explore the role of size for the composition towards $BiFeO_3$ side as well. Next chapter deals with the magnetic studies on BF-0.25PT sample and the effect of size on that.